Transverse-electric surface plasmon polaritons in periodically modulated graphene

Zeeshan Ahmad, Sang Soon Oh, and Egor A. Muljarov*
School of Physics and Astronomy, Cardiff University, Cardiff CF24 3AA, United Kingdom

(Received 8 February 2023; revised 22 January 2024; accepted 1 March 2024; published 20 May 2024)

Transverse-electric (TE) surface plasmon polaritons are unique eigenmodes of a homogeneous graphene layer that are tunable with the chemical potential and temperature. However, as their dispersion curve spectrally lies below the light line, they cannot be resonantly excited by an externally incident wave. Here, we propose a way of exciting the TE modes and tuning their peaks in the transmission by introducing a one-dimensional graphene grating. Using the scattering-matrix formalism, we show that periodic modulation of graphene makes transmission more pronounced, potentially allowing for experimental observation of the TE modes. Furthermore, we propose the use of turbostratic graphene to enhance the role of the surface plasmon polaritons in optical spectra.

DOI: 10.1103/PhysRevResearch.6.023185

I. INTRODUCTION

Surface plasmon polaritons (SPPs) in graphene have been an interesting area of theoretical and experimental research especially with the possibility of supporting SPPs with transverse-electric (TE) polarization in a graphene layer [1]. More recently, TE SPPs were shown to exist in a homogeneous layer of graphene for an extended frequency range at nonzero temperature [2] using a complex-frequency approach that models an open system with temporal decay. Although the TE SPP frequency dispersion is very close to the light line due to the small magnitude of the conductivity of graphene, proportional to the fine-structure constant [1], TE SPPs cannot be resonantly excited by an externally incident light because their dispersion curve lies below the light line.

Graphene is known for its tunability of optical conductivity by application of suitable gate voltage that induces sufficiently low but finite chemical potential [3]. This is because the electronic transitions occur near the K point [4], where the electronic dispersion is linear and the density of states vanishes. Devices like optical modulators [5] and polarizers [6], as well as absorption enhancement devices [7,8], benefit from this tunability, which, together with the existence of TE SPPs in graphene, provides exciting prospects for plasmonic applications [9]. In addition, structures with periodic graphene open the possibilities of generating topological plasmonic states [10–13] when a magnetic field is applied. Periodic plasmonic structures of graphene [14–17] and even multilayer stacks of periodic graphene strips [18–22] have been already studied. The effect of stacking graphene-dielectric layers on the properties of transverse-magnetic (TM) SPPs has also been analyzed for up to ten graphene layers [23]. Although the periodic graphene grating structure has been studied for TM SPP modes [14,16], it has not been proposed for excitation and measurement of TE SPPs in graphene, to the best of our knowledge.

The finite-element and finite-difference time-domain methods have been employed in many studies of plasmonic structures [11,24–30] to investigate SPPs. These fully numerical approaches are usually suitable for treating electromagnetic systems of relatively small sizes, but suffer from an increase in computation time for larger samples, since they require discretization of Maxwell's equations in real space over entire samples. For larger samples and extended periodic systems, expanding fields into Fourier harmonics presents a more suitable approach [31]. One can approximate structural details by expanding the solutions to Maxwell's equations in the Fourier space [32], organizing the obtained solutions as coefficients of Bragg diffraction orders, which is more appropriate for an infinite system with translational symmetries presented in this work. Although studies exist that consider periodic modulation of graphene at the atomic scale [33], these are suitable for periods of the order of nanometers. For a modulation period of microns order, which is sufficiently large compared to the electronic wavelengths, we may approximate the optical conductivity of graphene as isotropic [34] and consider the periodic modulation on the order of wavelengths of electromagnetic waves.

In this paper, we theoretically show that the TE SPP modes can be excited by incident light with an angle close to normal incidence with the help of one-dimensional periodic modulation in graphene. We demonstrate the excitation of the TE SPP modes as pronounced dips in the zeroth Bragg diffraction order transmission spectra. We also show that the in-plane wave number of the transmission dips are tunable with the grating period. To enhance the transmission feature of the graphene grating, we propose the use of multilayer turbostratic graphene strips [35,36]. Note that the TE SPP mode excitation presented here is different from excitation in metallic gratings of TM SPP by TE-polarized light incident

*egor.muljarov@astro.cf.ac.uk

at a nonzero angle between the direction of incident light projected onto the grating plane and the grating direction [37–39], allowing a nonzero electric field component parallel to the grating direction, in this way coupling the radiation to the TM SPP. It is well known (see, e.g., Ref. [40]) that TE SPPs do not form on homogeneous surfaces of metals with the permittivity described by the Drude model. Here instead, the TE SPP mode arises due to the interband part of the conductivity of graphene [1,2,41], where the electric field is always parallel to the graphene surface, and has no component in the grating direction.

To obtain the transmission spectra showing features due to the TE SPP modes, we employ the scattering-matrix formalism [42,43] that is commonly used for systems periodically modulated in space. The fact that the width of single- or multiple-layer graphene is much smaller than the SPP wavelength allows us to obtain an explicit analytical expression for the scattering matrix. The SPP modes, which are the eigensolutions of Maxwell's equations satisfying outgoing wave boundary conditions, correspond to the poles of the scattering matrix for the grating system [43,44] and manifest themselves as peaks and/or dips in transmission spectra. We have developed an analytical approximation for the scattering matrix, eigenmodes, and transmission, providing a proof that the features observed in optical spectra of periodically modulated graphene are in fact a manifestation of the TE SPP modes, which are unique to this kind of material.

II. THEORETICAL MODEL

In this section, we first derive, in the spirit of the scattering-matrix formalism [43], the transmission coefficients for a system containing an infinitesimally thin layer of a periodically modulated dispersive material surrounded by vacuum. Generalizations of the presented method to two-dimensional (2D) periodic modulation of an infinitesimally thin material layer and to systems with a substrate and/or superstrate are straightforward. The developed general formalism is applied to a one-dimensional periodic array of single- and multiple-layer graphene strips, by using the available analytic expression for the conductivity of graphene. We also present here a useful approximation of the transmission at normal incidence, valid for the frequencies near the crossing point of the folded SPP mode dispersion, which allows us to analyze the optical response of the periodically modulated system in terms of its SPP modes.

In the following, we use the model of the permittivity which is described in the entire space as

$$\varepsilon(x, z; \omega) = 1 + \chi(\omega)\Lambda(x)\delta(z), \tag{1}$$

where $\chi(\omega)$ is the 2D susceptibility of the infinitesimal layer, $\Lambda(x) = \Lambda(x + d)$ is a periodic function with period d describing the spatial modulation of the layer, and $\delta(z)$ is the Dirac delta function approximating the system as an infinitesimally thin layer. An illustration of the system studied in this work, which is a periodic array of graphene strips, as well as the geometry of the electromagnetic field in the TE polarization are shown in Fig. 1(a). The use of the Dirac delta function is justified by the condition that the graphene thickness is much smaller than the wavelength of the electromagnetic field.

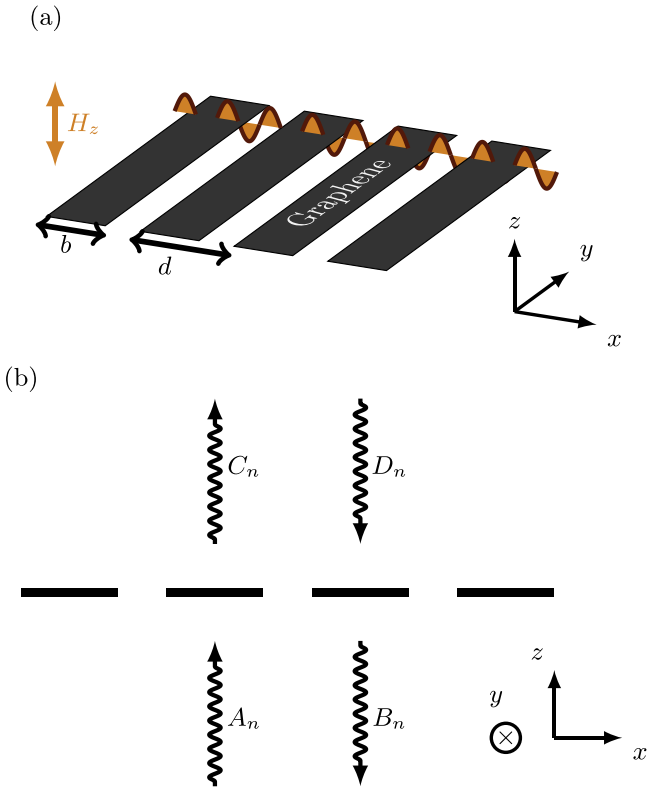

FIG. 1. Schematic of a graphene grating (a) in a perspective view and (b) in the xz-plane side view. An infinitesimally thin graphene layer at $z = 0$ is periodically modulated along the x axis but homogeneous along the y axis. Arrows labeled A_n, B_n, C_n, and D_n schematically represent incoming or outgoing coefficients of diffracted plane waves with an angle of incidence not necessarily normal.

A. Scattering matrix, transmission, and the eigenmodes of an infinitesimally thin periodically modulated layer

The scattering matrix, transmission and reflection coefficients, as well as the secular equation determining the dispersion of SPP modes are obtained in this section by solving Maxwell's equations,

$$\nabla \times \mathbf{E} = i\omega\mathbf{H}, \tag{2}$$

$$\nabla \times \mathbf{H} = -i\omega\varepsilon\mathbf{E}, \tag{3}$$

in which we assume nonmagnetic materials and use the units in which the speed of light $c = 1$. We also assume a harmonic time dependence of the electromagnetic field in the form of $e^{-i\omega t}$ and use the frequency- and position-dependent permittivity $\varepsilon(x, z; \omega)$ introduced in Eq. (1). For the zero component of the light wave number in the y direction, solutions of Maxwell's equations (2) and (3) split into TE and TM polarizations. We focus below on the TE polarization. The case of TM polarization for the same system is addressed in Appendix A 3.

For TE-polarized waves propagating in the x direction [Fig. 1(a)] with the wave number q, the magnetic and electric

fields in Cartesian coordinates take the form

$$\mathbf{H} = \begin{pmatrix} H_x \\ 0 \\ H_z \end{pmatrix}, \quad \mathbf{E} = \begin{pmatrix} 0 \\ E_y \\ 0 \end{pmatrix}, \tag{4}$$

respectively. The periodic grating profile $\Lambda(x)$ can be written as a Fourier series,

$$\Lambda(x) = \sum_n V_n e^{ig_n x}, \tag{5}$$

where

$$g_n = \frac{2\pi n}{d} \tag{6}$$

are the reciprocal lattice vectors and V_n are Fourier coefficients of the periodic function $\Lambda(x)$. We can take the general electric-field solution to Eqs. (2) and (3) in the basis of the same Fourier harmonics,

$$E_y(x,z) = \sum_n e^{i(q+g_n)x} \times \begin{cases} C_n e^{ik_n z} + D_n e^{-ik_n z}, & z > 0 \\ A_n e^{ik_n z} + B_n e^{-ik_n z}, & z < 0, \end{cases} \tag{7}$$

where A_n, B_n, C_n, and D_n are the field coefficients of the incoming and outgoing waves of Bragg order n, as depicted in Fig. 1(b). The normal component of the light wave number for each Bragg order is given by

$$k_n = \sqrt{\omega^2 - (q+g_n)^2}, \tag{8}$$

with the square root in Eq. (8) chosen in such a way that either $\mathrm{Re}\, k_n > 0$ or $\mathrm{Im}\, k_n > 0$, for any real frequency ω and real wave number q, so the term $C_n e^{ik_n z}$ in Eq. (7) describes, respectively, either a wave purely propagating in the z direction or a purely evanescent wave. For complex frequencies, the choice of the square root is determined by a proper analytic continuation of Eq. (8) from the real ω axis into the complex frequency plane. Note that the system has translational invariance, meaning that the wave number q as a real quantity is conserved (in periodic systems, up to the reciprocal Bragg vector g_n), making it a good quantum number. We therefore use here a real-valued in-plane wave number q allowing the mode eigenfrequency to be complex, as in our previous work [2]. This approach is widely used in the literature [43–45].

Integrating Eqs. (2) and (3) across the infinitesimal grating layer results in an infinite set of simultaneous equations for the amplitudes A_n, B_n, C_n, and D_n:

$$ik_n(C_n - D_n - A_n + B_n) = -\omega^2 \chi(\omega) \sum_m V_{n-m}(A_m + B_m),$$

$$C_n + D_n = A_n + B_n. \tag{9}$$

See Appendix A for a derivation.

Equations (9) can be written in matrix form as

$$\begin{pmatrix} \mathbf{C} \\ \mathbf{B} \end{pmatrix} = \mathbb{S} \begin{pmatrix} \mathbf{D} \\ \mathbf{A} \end{pmatrix}, \tag{10}$$

where $\mathbb{S}$ is the scattering matrix, and $\mathbf{A}$, $\mathbf{B}$, $\mathbf{C}$, and $\mathbf{D}$ are vectors containing the field coefficients A_n, B_n, C_n, and D_n, respectively. The scattering matrix can be expressed as

$$\mathbb{S} = \begin{bmatrix} -\mathbf{W}^{-1}\mathbf{U} & \mathbf{W}^{-1} \\ \mathbf{W}^{-1} & -\mathbf{W}^{-1}\mathbf{U} \end{bmatrix}, \tag{11}$$

where $\mathbf{W}^{-1}$ is the matrix inverse of $\mathbf{W} = \mathbf{I} + \mathbf{U}$, $\mathbf{I}$ is the identity matrix, and $\mathbf{U}$ is the matrix describing the coupling between diffraction orders, with the matrix elements given by

$$U_{nm} = \frac{\omega^2 \chi(\omega)}{2ik_n} V_{n-m}. \tag{12}$$

See Appendix A for details.

For any Bragg order n, the transmission coefficient T_n is given by the ratio of the energy of the diffracted wave of order n to the energy of an incoming wave (corresponding to $n = 0$), which can both be evaluated from the normal component of the Poynting vector [43], which yields

$$T_n = \left| \frac{k_n}{k_0} C_n^2 \right|. \tag{13}$$

Here, it is assumed without loss of generality that

$$A_n = \delta_{n0}, \quad D_n = 0, \tag{14}$$

where δ_{nm} is the Kronecker delta, and the expansion coefficients C_n in Eq. (13) are found by solving the linear algebraic equations (10) [or Eq. (9)] with the boundary conditions (14). Note that the above definition of the transmission coefficients, Eq. (13), is valid for so-called open diffraction channels only, for which

$$\omega^2 > (q + g_n)^2, \tag{15}$$

equivalent to k_n being real [see Eq. (8)]. For "closed" channels, inequality (15) is not fulfilled, and the values of T_n correspond to the near-field coefficients for these Bragg orders.

All the electromagnetic modes of the system, including the SPP modes and their dispersion relations, i.e., the dependence of the mode frequency on the wave number q, can be found from Eq. (10) by applying the outgoing boundary conditions, $\mathbf{A} = \mathbf{D} = 0$, for all Bragg orders. This is equivalent to solving a secular equation

$$\mathrm{Det}[\mathbb{S}^{-1}(\omega; q)] = 0, \tag{16}$$

or finding the poles of the scattering matrix $\mathbb{S}(\omega; q)$ in the complex frequency plane for any real wave number q.

B. Graphene conductivity and normalized frequencies and wave numbers

While the general method introduced in Sec. II A is suitable for treating any infinitesimally thin periodically modulated layer, in what follows, we consider a graphene grating structure depicted in Fig. 1. In this case, the susceptibility is given by [2]

$$\chi(\omega) = \frac{2iN\sigma(\omega)}{\omega}, \tag{17}$$

where $\sigma(\omega)$ is the 2D conductivity of a single homogeneous graphene layer and N is the number of parallel graphene layers stuck together in such a way that, on the one hand, the total thickness of the system is much smaller than the SPP wavelength, but on the other hand, all the layers are electronically decoupled and periodically modulated with the modulation function $\Lambda(x)$, the same for all layers. For the graphene strips shown in Fig. 1, we take this periodic function in the

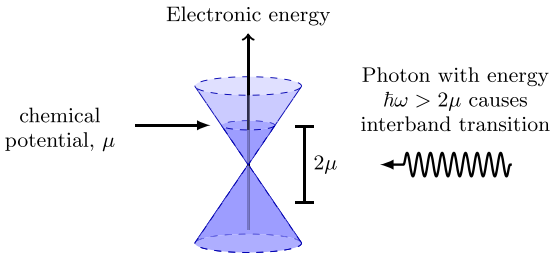

FIG. 2. Electronic dispersion, shown as electronic energy versus two-dimensional electronic momentum, of graphene near the K point with nonzero chemical potential μ and zero temperature. The darker colored region of surface of cone depicts energies occupied by charge carriers.

following form:

$$\Lambda(x) = \sum_n \Theta\left(\frac{b}{2} - |x - nd|\right), \tag{18}$$

where $\Theta(x)$ is the Heaviside step function and b is the width of the graphene strips.

In the long-wavelength limit, the single-layer frequency-dependent optical conductivity of graphene $\sigma(\omega)$ is presented in Refs. [1,41]. It is dependent on the Fermi-Dirac distribution function of charge carriers in graphene, which in turn depends on the electronic temperature $T_{\rm el}$ introduced at the microscopic level (see Appendices A and B in Ref. [2]). The conductivity is shown in Fig. 3(a) for zero temperature for graphene. In terms of the notations used in Ref. [2], the conductivity is given by

$$\sigma(\omega) = 2\pi[\sigma_{\rm intra}(\omega) + \sigma_{\rm inter}(\omega)], \tag{19}$$

and full expressions for $\sigma_{\rm intra}$ and $\sigma_{\rm inter}$, the intraband and interband parts of the graphene conductivity, are derived in Ref. [2]. While the intraband part, given by the Drude model, describes the physical mechanism of conductivity typical for normal metals, the interband part can be understood from the electronic band structure of graphene for a finite chemical potential μ, as shown in Fig. 2. The interband part $\sigma_{\rm inter}$ comes from optical transitions with energy greater than 2μ, contributing to a steplike feature in the real part of the conductivity, $\mathrm{Re}\,\sigma$, at $\mathrm{Re}\,\Omega = 2$, which can be seen in Fig. 3(a). The real part of the conductivity has the meaning of absorption having nonzero values at zero temperature only for frequencies greater than twice the chemical potential $\mathrm{Re}\,\Omega > 2$, with no interband absorption taking place for $\mathrm{Re}\,\Omega < 2$. There is also a dip in $\mathrm{Im}\,\sigma$ at $\mathrm{Re}\,\Omega = 2$ as shown in Fig. 3(a), consistent with the aforementioned steplike feature in $\mathrm{Re}\,\sigma$ and arising due to the Kramers-Kronig relations of conductivity as a response function. This dip is responsible for the enhancement of TE SPP features in transmission spectra presented in Sec. III.

Here and below we use for convenience dimensionless frequencies and wave numbers, all normalized to the chemical potential μ as

$$\Omega = \frac{\hbar\omega}{\mu}, \quad Q = \frac{\hbar q}{\mu}, \quad G_n = \frac{\hbar g_n}{\mu}, \quad K_n = \frac{\hbar k_n}{\mu}. \tag{20}$$

Equation (8) then modifies to $K_n = \sqrt{\Omega^2 - (Q + G_n)^2}$, and similar changes are made in all other equations. The periodicity of the structure generates the first Brillouin zone with the range $Q \in [-G_1/2, G_1/2]$, as depicted in Fig. 3(b). The conductivity $\sigma(\omega)$ is then called below $\sigma(\Omega)$, which is a function of the normalized frequency Ω, but it also depends on a normalized inverse temperature $\mu\beta = \mu/k_B T_{\rm el}$, where k_B is the Boltzmann constant.

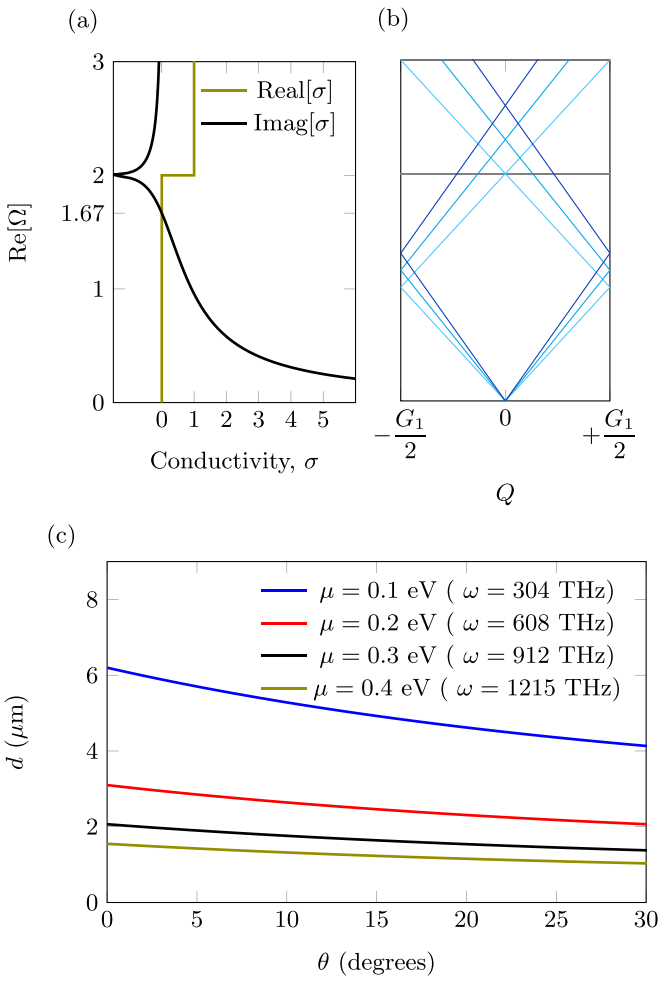

FIG. 3. (a) Conductivity of graphene at zero temperature ($T = 0$), sharing the frequency axis with dispersion in (b). The frequency of the interband dip in imaginary part of conductivity is affected by μ but not d. (b) Real part of the frequency of the TE mode dispersion of the homogeneous graphene structure folded into the first Brillouin zone, shown for $G_1 = 2$, 2.3, and 2.6 (thin, medium and thick blue lines, respectively). The size of the first Brillouin zone, and consequently the frequency of mode crossing at $Q = 0$, is controlled by μd. The TE mode frequency is close to the light line due to small value of the fine-structure constant. (c) The period of grating, d, required for normalized frequency $\Omega = 2$, various chemical potentials μ, and corresponding frequencies ω (legend) as a function of desired incidence angle $\theta = \arcsin(q/\omega)$ in degrees, using Eq. (21).

Let us note finally that multilayer graphene structures generally have interlayer coupling which alters the electronic band structure near the K point and thus qualitatively changes the optical conductivity spectrum. However, it is known that turbostratically stacked graphene layers have negligible interlayer coupling [46], simply factorizing the graphene conductivity [36]. Such graphene stacks have already been

synthesized [35,47]. We propose to use turbostratic multilayer graphene strips [48] to enhance features in transmission due to the TE SPP mode, including the increase of its linewidth and the frequency gap in the SPP mode dispersion. In this work, we obtain transmission spectra and approximate frequencies of the TE modes for both single-layer ($N = 1$) and turbostratic ($N = 10$) graphene grating by using the suitable number of graphene layers, N, in Eq. (17).

C. Controlling mode frequency and wave number

The conductivity spectrum of graphene has a key frequency $\mathrm{Re}\,\Omega = 2$ where the interband dip occurs in the imaginary part of the conductivity at low temperatures [see Fig. 3(a)]. Since the scattering matrix depends on frequency $\omega = \mu\Omega/\hbar$ and the SPP mode coupling due to the periodic modulation of the system depends on the grating period d, one can control this coupling and the SPP mode properties by varying the chemical potential μ and the period d. In fact, by tuning the grating period d, the edge of the first Brillouin zone $G_1/2$ where the bands are folded also changes, leading to variations of the frequency of the TE SPP folded mode crossing at $Q = 0$, as is clear from Fig. 3(b). Within and above the micrometer range, the grating period has a negligible effect on the conductivity spectrum, since the photon wave numbers in this case are much smaller than the electronic wave numbers [2]; this regime of a negligible spatial dispersion is described above as the long-wavelength limit of the conductivity. One can therefore independently choose a particular part of the conductivity spectrum shown in Fig. 3(a) and the desired normalized coupled mode frequency where the two TE SPP dispersion lines (which are close to the light lines) cross. For a better description of this tuning process, we define the normalized interband detuning $\Delta = G_1 - 2$, between the crossing in dispersion at $\Omega = G_1 = 2\pi\hbar/(\mu d)$ and the interband dip in the imaginary part of conductivity at $\Omega = 2$ as illustrated in Fig. 3(a). As an example, for a chemical potential of $\mu = 0.2$ eV, zero detuning ($\Delta = 0$) would require the graphene stripe width to be on the order of micrometers. Since the dispersion of the TE mode is close to the light line [1,2], we may approximate the TE mode dispersion as the folded light line and estimate the grating period required to tune the TE mode to a desired frequency Ω, for any in-plane wave number Q. In Fig. 3(c) we show the dependence of the grating period d required for the TE SPP mode of the $n = -1$ diffraction order to reach the frequency $\Omega = 2$. For general Ω and Q this condition is given by

$$d = \frac{\hbar}{\mu}\frac{2\pi}{\Omega + Q}. \tag{21}$$

Note that this dependence is shown in Fig. 3(c) in terms of different values of the chemical potential μ in eV, unnormalized frequency ω in hertz, and the angle of incidence, θ, measured from the normal to the graphene plane and defined as $\sin\theta = Q/\Omega$. Clearly $|\theta| \leqslant 30^\circ$ in this case, since $\Omega = G_1$ and $|Q| \leqslant G_1/2$ within the first Brillouin zone.

D. Role of the TE SPP modes in the transmission: Analytic approximation at normal incidence

To reveal the effects of periodic modulation on TE SPP modes and the role of these modes in the transmission, we focus in this section on the normal incidence and develop approximate analytical expressions for the transmission around the frequency $\mathrm{Re}\,\Omega = G_1$. To do so, we truncate $\mathbf{W}$ in the scattering matrix [Eq. (11)] to the lowest three diffraction orders, $n = 0$ and $n = \pm 1$:

$$\mathbf{W} = \begin{pmatrix} 1 + \frac{\Omega\tilde{V}_0}{K_{-1}} & \frac{\Omega\tilde{V}_{-1}}{K_{-1}} & \frac{\Omega\tilde{V}_{-2}}{K_{-1}} \\ \frac{\Omega\tilde{V}_1}{K_0} & 1 + \frac{\Omega\tilde{V}_0}{K_0} & \frac{\Omega\tilde{V}_{-1}}{K_0} \\ \frac{\Omega\tilde{V}_2}{K_1} & \frac{\Omega\tilde{V}_1}{K_1} & 1 + \frac{\Omega\tilde{V}_0}{K_1} \end{pmatrix}, \tag{22}$$

where $\tilde{V}_n = N\sigma(\Omega)V_n$ and $K_n \equiv \sqrt{\Omega^2 - (Q + G_n)^2}$.

The transmission amplitudes $t_n (t_n = C_n$ assuming $A_n = \delta_{n0}$ and $D_n = 0)$, related to the transmission coefficients T_n defined in Eq. (13) as $T_n = |K_n t_n^2/K_0|$, are then given by the middle column entries of $\mathbf{W}^{-1}$,

$$t_{\pm 1} = \frac{F_{\pm 1}}{|\mathbf{W}|}, \quad t_0 = \frac{F_0}{|\mathbf{W}|}, \tag{23}$$

where

$$F_{\pm 1} = \frac{\Omega^2}{K_1 K_{-1}}\tilde{V}_{\mp 1}\tilde{V}_{\pm 2} - \left(1 + \frac{\Omega}{K_{\mp 1}}\tilde{V}_0\right)\frac{\Omega}{K_{\pm 1}}\tilde{V}_{\pm 1}, \tag{24}$$

$$F_0 = \left(1 + \frac{\Omega}{K_{-1}}\tilde{V}_0\right)\left(1 + \frac{\Omega}{K_1}\tilde{V}_0\right) - \frac{\Omega^2}{K_1 K_{-1}}\tilde{V}_2\tilde{V}_{-2}, \tag{25}$$

and the determinant of Eq. (22) is given by

$$|\mathbf{W}| = \left(1 + \frac{\Omega}{K_0}\tilde{V}_0\right)F_0 + \frac{\Omega}{K_0}\tilde{V}_1 F_{-1} + \frac{\Omega}{K_0}\tilde{V}_{-1}F_1. \tag{26}$$

Note that the modulated TE SPP mode frequencies correspond to the zeros of this determinant.

For $Q = 0$, corresponding to normal incidence, the approximate transmission amplitudes obtained in Eq. (23) can be further simplified by using the fact that $K_0 = \Omega$ and $K_{\pm 1} = \sqrt{\Omega^2 - G_1^2}$, which results in

$$F_{\pm 1} = -\frac{\Omega\tilde{V}_1}{K_1}\mathcal{D}_-(\Omega), \tag{27}$$

$$F_0 = \mathcal{D}_-(\Omega)\,\mathcal{D}_+(\Omega), \tag{28}$$

$$|\mathbf{W}| = \mathcal{D}_-(\Omega)\,\mathcal{B}(\Omega), \tag{29}$$

where

$$\mathcal{D}_\pm(\Omega) = 1 + \frac{\Omega}{K_1}(\tilde{V}_0 \pm \tilde{V}_2), \tag{30}$$

and

$$\mathcal{B}(\Omega) = 1 + \tilde{V}_0 + \frac{\Omega}{K_1}\left[\tilde{V}_0 + \tilde{V}_2 + \tilde{V}_0(\tilde{V}_0 + \tilde{V}_2) - 2\tilde{V}_1^2\right]. \tag{31}$$

Here, without loss of generality, we have made use of the fact that the Fourier coefficients V_n of the grating profile function $\Lambda(x)$ are real, if $\Lambda(x)$ is an even function of x; therefore, $\tilde{V}_n = \tilde{V}_{-n}$. Thus, for $Q = 0$, the transmission amplitudes in Eq. (23) reduce to

$$t_0(\Omega) = \frac{\mathcal{D}_+(\Omega)}{\mathcal{B}(\Omega)}, \quad t_{\pm 1}(\Omega) = -\frac{\Omega}{K_1}\frac{\tilde{V}_1}{\mathcal{B}(\Omega)}. \tag{32}$$

As it is clear from Fig. 3(b), the two folded dispersion lines originating from the unperturbed TE SPP of the homogeneous

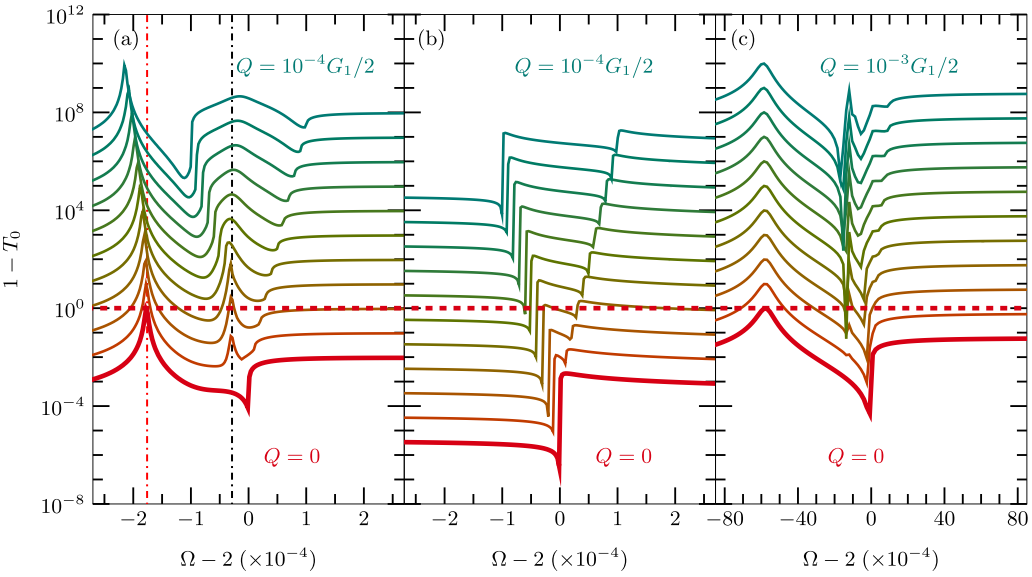

FIG. 4. Transmission spectra $(1 - T_0)$ for zeroth diffraction order (close-to-normal incidence) when a TE-polarized light with parallel wave number Q is incident on the grating with $b/d = 0.3$, $\Delta = 0$, for (a) single-layer graphene with $\sigma/2\pi = \sigma_{\text{intra}} + \sigma_{\text{inter}}$, (b) single-layer graphene without interband conductivity $\sigma/2\pi = \sigma_{\text{intra}}$, and (c) turbostratically stacked graphene with $\sigma/2\pi = N(\sigma_{\text{intra}} + \sigma_{\text{inter}})$, for $N = 10$. The dashed red line indicates $T_0 = 0$. Spectra for $Q \neq 0$ are offset by powers of 10 in increasing order of Q. Red and black vertical dash-dotted lines indicate the real parts of the bright and dark TE SPP resonance frequencies for $Q = 0$, which are solutions of Eqs. (34) and (33), respectively.

layer, corresponding to the $n = 1$ and $n = -1$ Bragg orders and crossing at $\Omega \approx G_1$, produce in a periodically modulated system two perturbed TE SPP modes at each Q. The frequencies of these modes can be found from the zeros of the determinant in Eq. (26), which factorizes at $Q = 0$, according to Eq. (29). One mode, having frequency Ω_d, is found from the condition $\mathcal{D}_-(\Omega_d) = 0$, which yields

$$\frac{\Omega_d}{G_1} = \frac{1}{\sqrt{1 - (\tilde{V}_0 - \tilde{V}_2)^2}}, \tag{33}$$

and is further referred to as the *dark mode*, as it does not manifest itself in the normal-incidence transmission. In fact, since $F_{\pm 1}$ and F_0 are proportional to $\mathcal{D}_-(\Omega)$ there is an exact cancellation of this factor in $t_{\pm 1}$ and t_0. The other mode, having frequency Ω_b, which we further call the *bright mode*, is obtained from equating to zero the other factor in $|\mathbf{W}|$ given by Eq. (29), $\mathcal{B}(\Omega_b) = 0$, which yields

$$\frac{\Omega_b}{G_1} = \frac{1 + \tilde{V}_0}{\sqrt{(1 + \tilde{V}_0)^2 - \left[(1 + \tilde{V}_0)(\tilde{V}_0 + \tilde{V}_2) - 2\tilde{V}_1^2\right]^2}}. \tag{34}$$

This mode does contribute to the transmission, which in turn can be approximated for the frequencies Ω close to Ω_b as

$$t_0(\Omega) \approx \frac{\mathcal{D}_+(\Omega_b) + (\Omega - \Omega_b)\mathcal{D}'_+(\Omega_b)}{(\Omega - \Omega_b)\mathcal{B}'(\Omega_b)}, \tag{35}$$

and a similar approximate expression can be obtained for $t_{\pm 1}(\Omega)$. While the $\tilde{V}_1^2$ term in Eq. (34) presents a higher-order correction (comparable to the contribution of all neglected Bragg orders) and results in a relative change of Ω_b of order 10^{-4}, it is significant for the zeroth-order transmission, otherwise the pole at the bright mode is exactly compensated by the numerator in t_0, as can be seen from Eqs. (30)–(32).

Note that Eqs. (33) and (34) are not explicit expressions for Ω_d and Ω_b respectively, but should instead be solved self-consistently, as the matrix elements $\tilde{V}_n$, even though small, are dependent on frequency through the conductivity $\sigma(\Omega)$. However, one can use $\Omega = G_1$ as a good starting value for a quickly converging self-consistent iterative solution of Eqs. (33) and (34), which is implemented in this work and illustrated in Sec. III.

Note also that in the absence of the periodic modulation $\tilde{V}_n = \delta_{n,0} N\sigma(\Omega)$, and both modes have exactly the same frequency, given by $\Omega_{b,d} = G_1/\sqrt{1 - \tilde{V}_0^2}$, which coincides with the homogeneous graphene dispersion [2] folded into the center of the first Brillouin zone.

III. RESULTS

We now present transmission spectra of periodically modulated graphene at $\mu\beta = 10^5$, with 30% filling factor ($b/d = 0.3$), for normal and close-to-normal incidence of a TE-polarized incoming plane wave. Here, the grating period d is chosen in such a way that $\Delta = 0$ (equivalent to $G_1 = 2$). For this grating period, the crossing point of the folded light dispersion at $Q = 0$ coincides with the interband dip in the imaginary part of the conductivity [see Figs. 3(a) and 3(b)]. It is therefore expected that the coupling of the TE SPP modes of a homogeneous graphene, which is caused by its periodic modulation, is maximized, and thus features in transmission due to the TE SPP modes are enhanced.

Figure 4 shows the transmission spectra in the zeroth diffraction order, $1 - T_0$, for single-layer graphene grating in Fig. 4(a), single-layer graphene grating without interband conductivity σ_{inter} in Fig. 4(b), and turbostratic ($N = 10$) graphene grating in Fig. 4(c), calculated with the scattering matrix truncated to the lowest 21 Bragg orders ($-10 \leqslant n \leqslant$

10). In all three cases, the first ($n = 1$) and minus-first ($n = -1$) Bragg order light lines are evident as dips in $1 - T_0$ that move away from each other almost linearly with Q, as Q increases starting from zero. When the contribution of the interband conductivity σ_{inter} is removed from the total conductivity σ, these dips are clearly seen in Fig. 4(b) in addition to a steplike feature also moving linearly with Q along the minus-first Bragg order light line. This steplike feature, also present in some form in the graphene transmission [Figs. 4(a) and 4(c)], is caused by opening the minus-first diffraction channel with increasing frequency in accordance with Eq. (15). Such features are common to the optical spectra of periodic systems [49,50].

The most important features in the spectra of periodically modulated graphene [Figs. 4(a) and 4(c)] are also highlighted by their comparison with the normal metal spectra [Fig. 4(b)]. These are peaks in $1 - T_0$ which appear also close to the folded light lines and are the manifestation of the TE SPP modes in periodically modulated graphene. At the frequencies of these TE SPP peaks, the energy of the incoming TE beam is diverted back into reflection, as demonstrated in Appendix B, showing in the same and in a much larger frequency range the transmission in zeroth and other ($n = \pm 1$) diffraction orders, as well as the absorption (see Figs. 9 and 12 for $\Delta = 0$; results for nonzero detuning Δ are also presented in Appendix B).

In the selected frequency range close to $\Omega = G_1$, one would expect to observe in Figs. 4(a) and 4(c) two TE SPP modes, separated by a frequency gap, in accordance with Fig. 3(b). This is a general property of planar photonic-crystal structures which is usually caused by guided-mode folding and their hybridization due to the coupling between Bragg orders [43,51,52]. However, for $Q = 0$, we see in Fig. 4(a) only one peak at around $\Omega - 2 \approx -1.76 \times 10^{-4}$. The second peak is missing for $Q = 0$ and appears only at nonzero values of Q. This is, however, in full agreement with our analysis of the transmission, presented in Sec. II D in terms of the bright and dark TE SPP modes. The real parts of their frequencies, Ω_b and Ω_d, are also shown in Fig. 4(a) by vertical dash-dotted lines, demonstrating a good agreement with the peak positions. The linewidth of the dark mode is increasing with Q, and both modes are deviating from their positions at $Q = 0$. We evaluate the frequency gap between the two TE SPP modes to be approximately 1.47×10^{-4}. Note that a similar behavior has been observed in transmission spectra of a distributed feedback microcavity structure [51,52] in which bright and dark modes originate from the interaction of the folded guided-mode dispersion lines.

A further analysis of the transmission spectrum at $Q = 0$ is presented in Fig. 5, which shows $1 - T_0$ calculated using the approximation (35) (red line) and the full scattering matrix truncated up to 21 Bragg orders (blue line), demonstrating a good agreement between the two near $\Omega \approx \Omega_b$ (vertical red dashed line). Away from Ω_b, the approximate transmission [Eq. (35)], based on the first-order Taylor expansion, naturally deviates from the exact result. This analysis provides a proof that the observed peaks in the transmission are in fact a manifestation of the TE SPP modes predicted in a homogeneous graphene layer [1,2]. However, in homogeneous systems, these modes spectrally lie below the light line and thus cannot be excited resonantly. By periodically modulating the homogeneous graphene layer, the TE SPP modes can be seen in optical spectra.

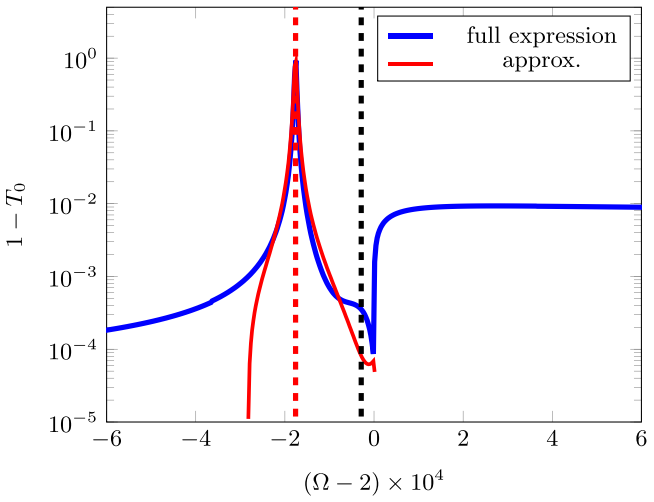

FIG. 5. Approximation of transmission (red solid line) using Eq. (35) showing consistency with the TE peak for $Q = 0$ and $\Delta = 0$ (blue solid line). Red and black dashed lines indicate the real part of the frequencies of the bright and dark TE SPP modes, obtained using Eq. (34) and Eq. (33), respectively. The frequency gap between the dashed lines is approximately 1.47×10^{-4}.

Using turbostratic graphene grating as shown in Fig. 4(c), TE mode peaks coming from interband conductivity can be further pronounced. Similar to the single-layer case, the main peak reaches its maximum value of 1. However, both the width of the peaks due to TE SPPs and their positions in frequency are affected by the use of turbostratic graphene. Note that the TE mode peak at $Q = 0$ has been shifted further away from the light line, about a factor of 35 more compared to its previous position for the single-layer case in Fig. 4(a). The peak has a larger full width at half maximum (FWHM), making TE SPP mode easier to detect. The peak frequency does not change much for Q close to zero, but eventually starts to shift to lower frequencies as Q is increased [this can be seen in Fig. 12(c) in Appendix B]. The dark TE SPP mode peak only appears for $Q \neq 0$ as seen in Fig. 4(c), similar to the single-layer case. However, it demonstrates a fine structure, consisting of multiple peaks, which is due to a stronger coupling between the TE SPP modes and higher Bragg orders more strongly contributing to the scattering matrix.

The effect of temperature T_{el} on the transmission spectrum is presented in Fig. 6 for $Q = 0$. Note that the dependence on T_{el} arises due to the interband conductivity of graphene, strongly dependent on temperature through the Fermi-Dirac distribution function as already discussed in Refs. [1,2,41]. It is evident from Fig. 4, comparing transmission spectra with and without the interband term of the conductivity, that interband conductivity is crucial for the formation of the TE mode; hence the transmission may strongly depend on temperature. In fact, increasing temperature smears the Fermi-Dirac distribution function, in turn smearing the interband conductivity function near $\Omega = 2$ [2]. Figure 6 shows that the TE mode peak is reaching its maximum height of 1 at zero temper-

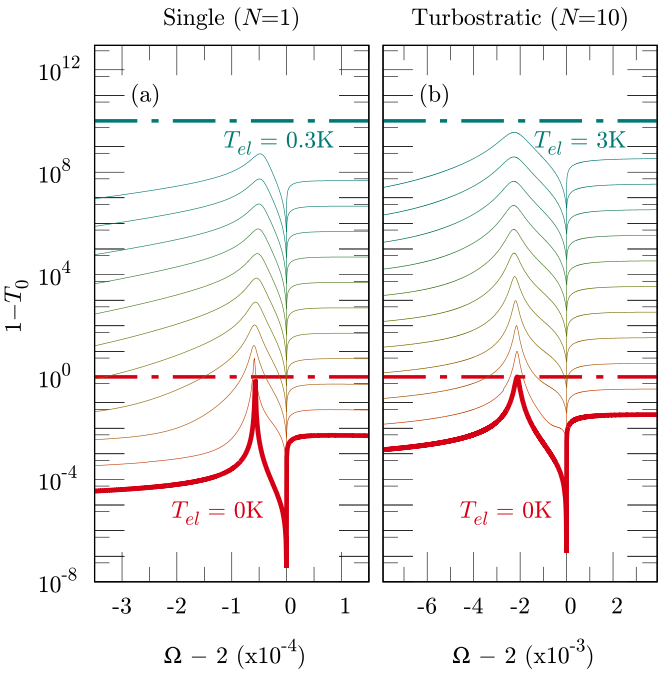

FIG. 6. Transmission spectra $(1 - T_0)$ for zeroth diffraction order when a TE-polarized light is normally incident ($Q = 0$) on grating with $b/d = 0.3$, for $\Delta = 0$, shown from zero temperature (red) to finite temperature (green), for (a) single-layer graphene and (b) turbostratically stacked graphene. Red and green dash-dotted lines indicate $T_0 = 0$ for zero temperature and $T_{\rm el} = 0.3$ K (single) or $T_{\rm el} = 3$ K (turbostratic), respectively.

ature in both the single-layer and turbostratic case. For the single-layer case, increasing temperature smears the peak out, with the peak maximum reduced. For the turbostratic case, the peak is still present at 3 K with minimal smearing. This reduced sensitivity of transmission to temperature suggests further in favor of turbostratic over single-layer graphene for applications using TE SPPs operating within the temperature range presented in Fig. 6(b).

To estimate a potential role of disorder in the transmission spectra of the system, we have evaluated the FWHM of the TE peak in the transmission of the periodically modulated turbostratic graphene in Fig. 4(c) at $b/d = 0.3$. We found that for up to 20% deviation of filling factor, a shifted TE SPP peak still lies within the original FWHM. Furthermore, in the case of turbostratic graphene, the FWHM is larger, making the TE mode more robust with respect to temperature changes.

IV. CONCLUSIONS

We have shown that the complex-frequency transverse-electric surface plasmon polariton (TE SPP) modes in a graphene grating can be excited by external electromagnetic waves with close-to-normal incidence. Specifically, a significant reduction in the zeroth diffraction order transmission is observed near the interband transition frequency of graphene. This reduction can be explained as a reflection of the energy of the incoming beam due to the resonant coupling to the TE SPP modes. In addition, we have shown that the frequency and the in-plane wave number of TE SPP modes seen in transmission can be tuned by controlling the graphene chemical potential and grating period. Specifically, we have demonstrated that for zero detuning, that is, the grating period is chosen so that the TE SPP mode energy matches the interband threshold of the graphene conductivity, the features in the optical spectra due to the TE SPPs are significantly enhanced. Furthermore, by using turbostratic graphene layers with negligible interlayer interactions, we can enhance these features further, making them experimentally more accessible than in the single-layer graphene.

The data that support the findings of this study are available in the Cardiff University Research Portal at Ref. [53].

ACKNOWLEDGMENTS

Z.A. acknowledges financial support of EPSRC under the DTP scheme (Grant No. EP/R513003/1). S.S.O. acknowledges the support of Sêr Cymru II Rising Star Fellowship [80762-CU145 (East)], which is partly funded by the European Regional Development Fund (ERDF) via the Welsh Government.

APPENDIX A: SCATTERING-MATRIX APPROACH

1. Solving Maxwell's equations for an infinitesimally thin periodic layer

We start from Maxwell's equations having the form

$$\nabla \times \mathbf{E} = -\partial_t \mathbf{H}, \tag{A1}$$

$$\nabla \times \mathbf{H} = \partial_t \mathbf{D}, \tag{A2}$$

where we assume nonmagnetic materials, i.e., the permeability $\mu = 1$ everywhere in space, and use the units in which the speed of light $c = 1$. Assuming a harmonic dependence on time of the electromagnetic field in the form of $e^{-i\omega t}$, we obtain

$$\nabla \times \mathbf{E} = i\omega \mathbf{H}, \tag{A3}$$

$$\nabla \times \mathbf{H} = -i\omega\varepsilon(\omega)\mathbf{E}. \tag{A4}$$

For the TE polarization, the magnetic and electric fields can be expressed in terms of their Cartesian components as

$$\mathbf{H} = \begin{pmatrix} H_x \\ 0 \\ H_z \end{pmatrix}, \quad \mathbf{E} = \begin{pmatrix} 0 \\ E_y \\ 0 \end{pmatrix}. \tag{A5}$$

Maxwell's equations then take the form

$$\begin{pmatrix} -\partial_z E_y \\ 0 \\ \partial_x E_y \end{pmatrix} = i\omega \begin{pmatrix} H_x \\ 0 \\ H_z \end{pmatrix}, \tag{A6}$$

$$\begin{pmatrix} \partial_y H_z \\ \partial_z H_x - \partial_x H_z \\ -\partial_y H_x \end{pmatrix} = -i\omega\varepsilon \begin{pmatrix} 0 \\ E_y \\ 0 \end{pmatrix}. \tag{A7}$$

These can be rewritten as

$$-\partial_z E_y = i\omega H_x, \tag{A8}$$

$$\partial_x E_y = i\omega H_z, \tag{A9}$$

$$\partial_z H_x - \partial_x H_z = -i\omega\varepsilon E_y. \tag{A10}$$

As defined in Eq. (1), the permittivity in the whole space is given by $\varepsilon(x, z; \omega) = 1 + \chi(\omega)\Lambda(x)\delta(z)$, where $\chi(\omega)$ is the 2D susceptibility of an infinitesimally thin layer and $\Lambda(x)$ is a periodic function describing its spatial modulation, which can be represented by its Fourier series as

$$\Lambda(x) = \sum_n V_n e^{ig_n x}. \tag{A11}$$

Integrating Eqs. (A8) and (A10) over z across the point $z = 0$, we obtain

$$-E_y|_{z=0^+} + E_y|_{z=0^-} = 0, \tag{A12}$$

$$H_x|_{z=0^+} - H_x|_{z=0^-} = -i\omega\chi(\omega)\Lambda(x)E_y|_{z=0}, \tag{A13}$$

where $0^{+(-)}$ is a positive (negative) infinitesimal. For the TE polarization, it is easier to eliminate H_x and write equations in terms of the E_y component having the following general form,

$$E_y(x, z) = \sum_n e^{i(q+g_n)x} \times \begin{cases} C_n e^{ik_n z} + D_n e^{-ik_n z}, & z > 0 \\ A_n e^{ik_n z} + B_n e^{-ik_n z}, & z < 0, \end{cases} \tag{A14}$$

in which g_n and k_n are defined, respectively, by Eqs. (6) and (8), and q is the wave number along x.

Substituting Eq. (A8) into Eq. (A13), we obtain

$$\partial_z E_y\big|_{z=0^+} - \partial_z E_y\big|_{z=0^-} = -\omega^2\chi(\omega)\Lambda(x)E_y\big|_{z=0}, \tag{A15}$$

which after using the series of Eqs. (A11) and (A14) becomes

$$\sum_n ik_n(C_n - D_n - A_n + B_n)e^{i(q+g_n)x} = -\omega^2\chi(\omega)\sum_{mn} e^{iqx}e^{ig_{m+n}x}V_m(A_n + B_n). \tag{A16}$$

By shifting the indices of summation $n \to n - m$ in the right-hand side of Eq. (A16), we find

$$\sum_n ik_n(C_n - D_n - A_n + B_n)e^{i(q+g_n)x} = -\omega^2\chi(\omega)\sum_{m,n} e^{iqx}e^{ig_n x}V_m(A_{n-m} + B_{n-m}), \tag{A17}$$

and then equating the coefficients at $e^{i(q+g_n)x}$ in Eq. (A17), we obtain

$$ik_n(C_n - D_n - A_n + B_n) = -\omega^2\chi(\omega)\sum_m V_m(A_{n-m} + B_{n-m}). \tag{A18}$$

Finally, shifting the indices again in the summation in Eq. (A18), by substituting $m \to -m + n$, we arrive at

$$ik_n(C_n - D_n - A_n + B_n) = -\omega^2\chi(\omega)\sum_m V_{n-m}(A_m + B_m). \tag{A19}$$

In addition to this, we find from the continuity of the electric field, Eq. (A12), that

$$C_n + D_n = A_n + B_n. \tag{A20}$$

An infinite set of simultaneous equations given by Eqs. (A19) and (A20) presents a general solution of Maxwell's equation in TE polarization for the infinitesimally thin periodically modulated layer.

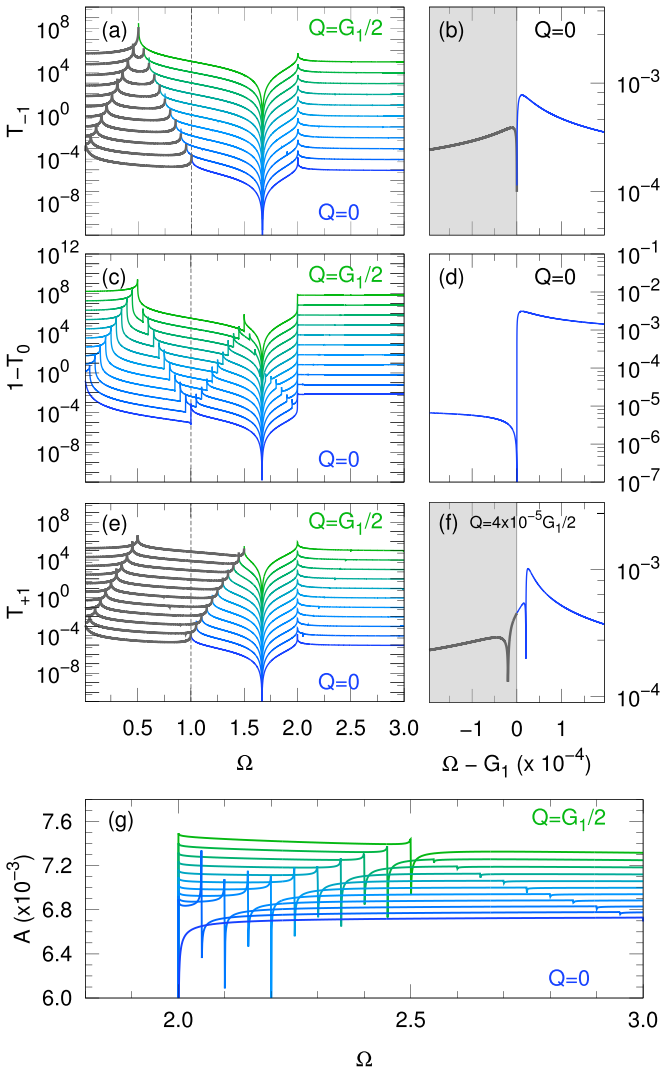

FIG. 7. Transmission spectra for single-layer graphene ($N = 1$), for the [(a), (b)] minus-first diffraction order, [(c), (d)] zeroth diffraction order, and [(e), (f)] first diffraction order, for the period d adjusted so that $\Delta = -1$ ($G_1 = 1$). Panels (b) and (d) zoom in the spectral features near $\Omega = G_1$ in (a) and (c), respectively, for $Q = 0$. (g) Absorption calculated using Eq. (B1), with waterfall increment of 0.02. $A(\Omega < 2) = 0$ for zero temperature. The gray solid lines correspond to the forbidden frequency range where Eq. (15) is not satisfied, and the curve has the meaning of the near-field amplitude.

2. Deriving the scattering matrix

To build a scattering matrix, let us rearrange Eqs. (A19) and (A20) in the following way:

$$C_n + B_n + \sum_m \frac{\omega^2\chi(\omega)}{ik_n}V_{n-m}B_m = A_n + D_n - \sum_m \frac{\omega^2\chi(\omega)}{ik_n}V_{n-m}A_m, \tag{A21}$$

$$C_n - B_n = A_n - D_n. \tag{A22}$$

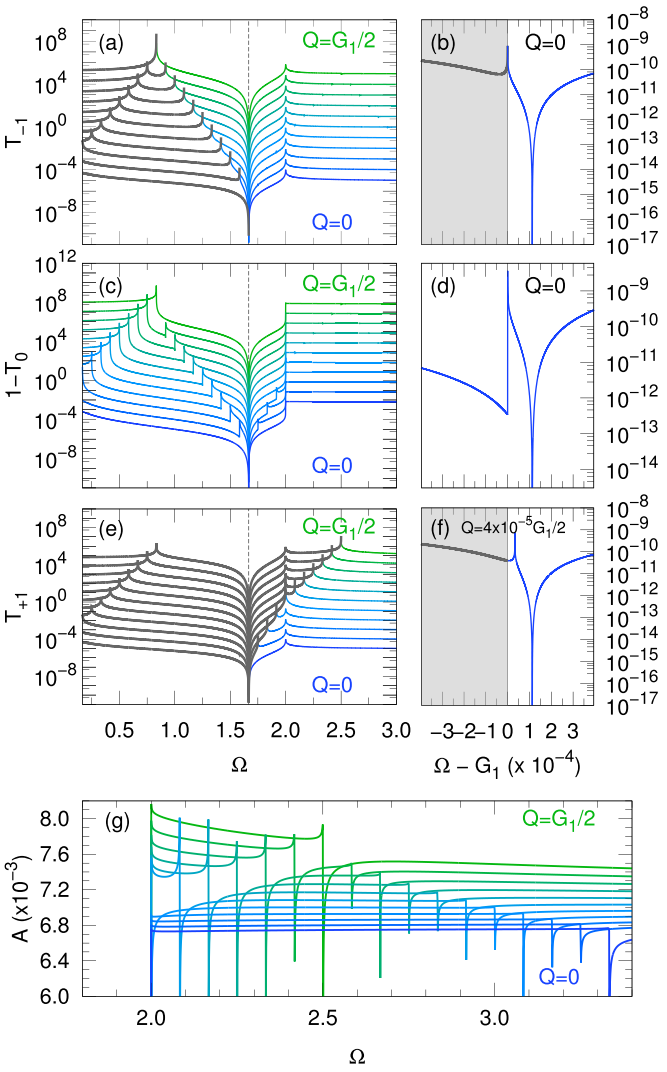

FIG. 8. As Fig. 7 but for $\Delta = -2 + 1.667$ ($G_1 = 1.667$), illustrating attenuation of near-field and transmission amplitudes.

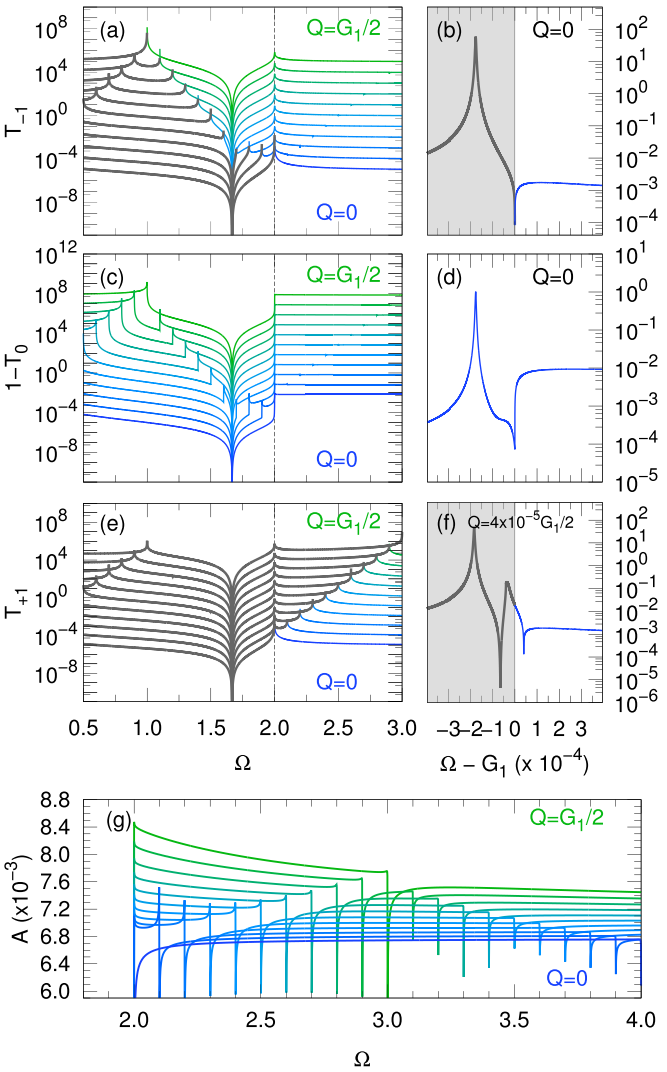

FIG. 9. As Fig. 7 but for $\Delta = 0$ ($G_1 = 2$), illustrating the amplification of the near-field and transmission amplitudes.

Thus, in terms of 2×2 matrices of Bragg-order blocks, Eqs. (A21) and (A22) can be written as

$$\begin{bmatrix} \mathbf{I} & \mathbf{I}+2\mathbf{U} \\ \mathbf{I} & -\mathbf{I} \end{bmatrix} \begin{bmatrix} \mathbf{C} \\ \mathbf{B} \end{bmatrix} = \begin{bmatrix} \mathbf{I} & \mathbf{I}-2\mathbf{U} \\ -\mathbf{I} & \mathbf{I} \end{bmatrix} \begin{bmatrix} \mathbf{D} \\ \mathbf{A} \end{bmatrix}, \tag{A23}$$

where vectors $\mathbf{A}$, $\mathbf{B}$, $\mathbf{C}$, and $\mathbf{D}$ have components A_n, B_n, C_n, and D_n, respectively, matrix $\mathbf{U}$ has the matrix elements

$$U_{nm} = \frac{\omega^2 \chi(\omega)}{2ik_n} V_{n-m}, \tag{A24}$$

and $\mathbf{I}$ is the identity matrix.

The scattering matrix, relating the amplitudes of incoming and outgoing waves, is then given by

$$\mathbb{S} = \begin{bmatrix} \mathbf{I} & \mathbf{I}+2\mathbf{U} \\ \mathbf{I} & -\mathbf{I} \end{bmatrix}^{-1} \begin{bmatrix} \mathbf{I} & \mathbf{I}-2\mathbf{U} \\ -\mathbf{I} & \mathbf{I} \end{bmatrix}. \tag{A25}$$

To further simplify it, we can write the inverse of the square matrix in Eq. (A25) in terms of its blocks:

$$\mathbb{S} = \frac{1}{2} \begin{bmatrix} \mathbf{W}^{-1} & \mathbf{W}^{-1}(\mathbf{I}+2\mathbf{U}) \\ \mathbf{W}^{-1} & -\mathbf{W}^{-1} \end{bmatrix} \begin{bmatrix} \mathbf{I} & \mathbf{I}-2\mathbf{U} \\ -\mathbf{I} & \mathbf{I} \end{bmatrix}, \tag{A26}$$

where $\mathbf{W} = \mathbf{I} + \mathbf{U}$. Finally, performing the matrix multiplication, we obtain

$$\mathbb{S} = \begin{bmatrix} -\mathbf{W}^{-1}\mathbf{U} & \mathbf{W}^{-1} \\ \mathbf{W}^{-1} & -\mathbf{W}^{-1}\mathbf{U} \end{bmatrix}. \tag{A27}$$

3. TM polarization

We note that TM polarization can be treated in exactly the same manner as the TE polarization solved above, leading to the same form as Eq. (A27) for the scattering matrix, provided that the matrix $\mathbf{U}$ is replaced with $\mathbf{U}^{\mathrm{TM}}$ having the matrix elements

$$U^{\mathrm{TM}}_{nm} = -\tfrac{1}{2} ik_n \chi(\omega) V_{n-m}. \tag{A28}$$

Also, in TM polarization, the vectors $\mathbf{A}$, $\mathbf{B}$, $\mathbf{C}$, and $\mathbf{D}$ have the same meaning as the expansion coefficients in Eq. (A14), but for $H_y(x, z)$ instead, which in this case is the only nonzero component of the magnetic field.

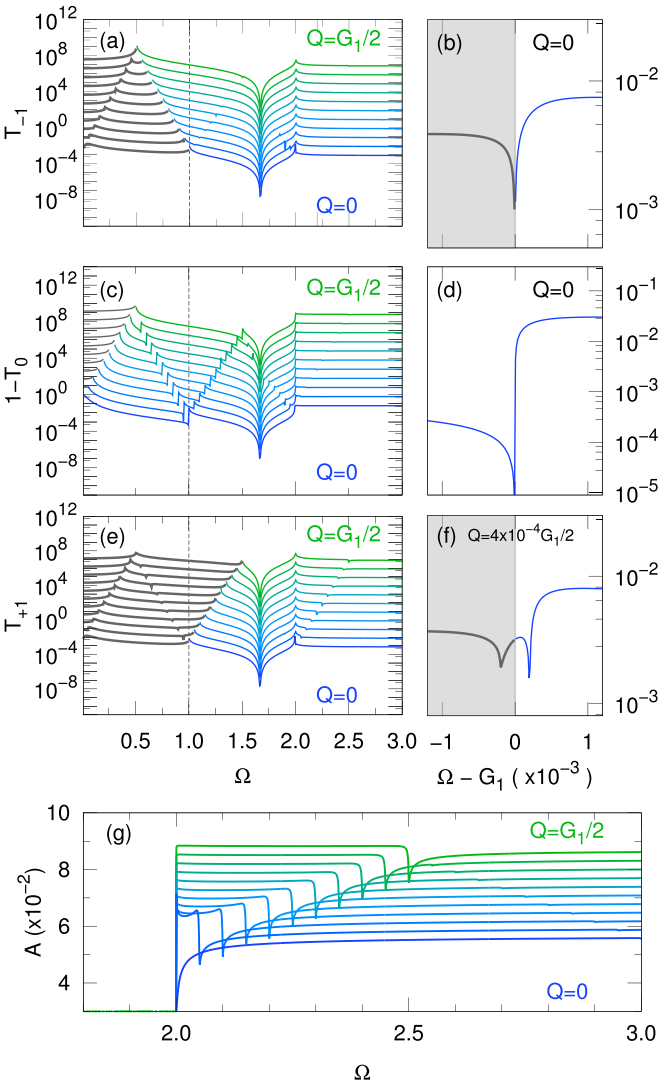

FIG. 10. Transmission spectra for turbostratic ($N = 10$) graphene, for the [(a), (b)] minus-first diffraction order, [(c), (d)] zeroth diffraction order, and [(e), (f)] first diffraction order for detuning $\Delta = -1$ ($G_1 = 1$). Panels (b) and (d) zoom in the spectral features near $\Omega = G_1$ in (a) and (c), respectively, for $Q = 0$. Similarly, panel (f) is a zoom in of panel (e) at Q close to but not zero. Gray regions and curves indicate forbidden frequency regions. (g) Absorption spectrum obtained using Eq. (B1), with waterfall increment of 0.2.

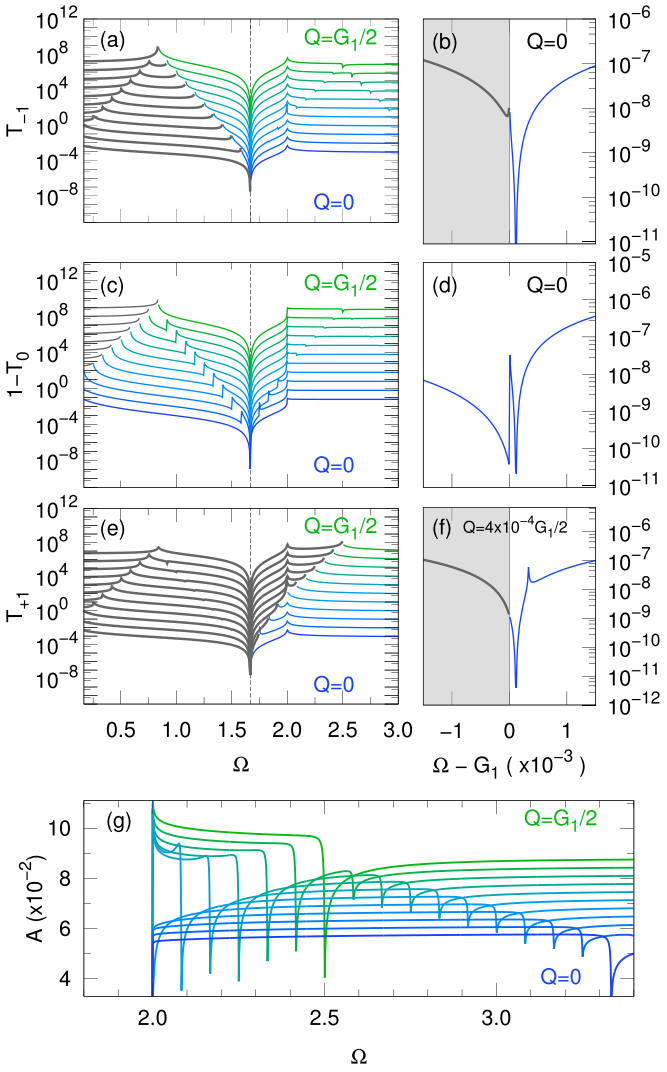

FIG. 11. As Fig. 10 but for $\Delta = -2 + 1.667$ ($G_1 = 1.667$).

APPENDIX B: TRANSMISSION AND ABSORPTION SPECTRA

Here we present the transmission spectra, calculated using Eq. (13), for grating with the filling factor $b/d = 0.3$ for $Q \in [0, G_1/2]$ and for different grating periods such that $\Delta = -1$, $-2 + 1.667$, and 0. We also show the absorption defined as

$$A(\Omega) = 1 - \sum_{n\in\{\Omega>|Q+G_n|\}} [T_n(\Omega) + R_n(\Omega)], \qquad \text{(B1)}$$

where

$$R_n(\Omega) = \left|\frac{k_n}{k_0} B_n^2\right| \qquad \text{(B2)}$$

is the reflection coefficient of the nth diffraction order. Note that the summation in Eq. (B1) is performed over open diffraction channels only, satisfying the condition in Eq. (15), as indicated in the formula.

1. Single-layer case

Figures 7–9 show transmission and absorption spectra for single-layer ($N = 1$) graphene grating for $\Delta = -1$, $-2 + 1.667$, and 0, respectively, corresponding to $G_1 = 1$, 1.667, and 2.

The SPP modes manifest themselves as peaks in the transmission spectra in Figs. 7(a), 7(c), and 7(e) (and corresponding panels in Figs. 8 and 9), and as dips in Figs. 7(g), 8(g), and 9(g), all moving almost linearly with Q. The absorption A in Figs. 7(g), 8(g), and 9(g) is zero for $\Omega < 2$ and is about 10^{-2} otherwise, which correlates with the interband absorption having a sharp frequency cutoff at $\Omega = 2$ for zero temperature. In the zeroth order transmission $1 - T_0$, the TE SPP mode peaks are lost due to the stronger interband absorption for frequencies above $\Omega > 2$, instead appearing as dips in the absorption spectrum A, for such frequencies.

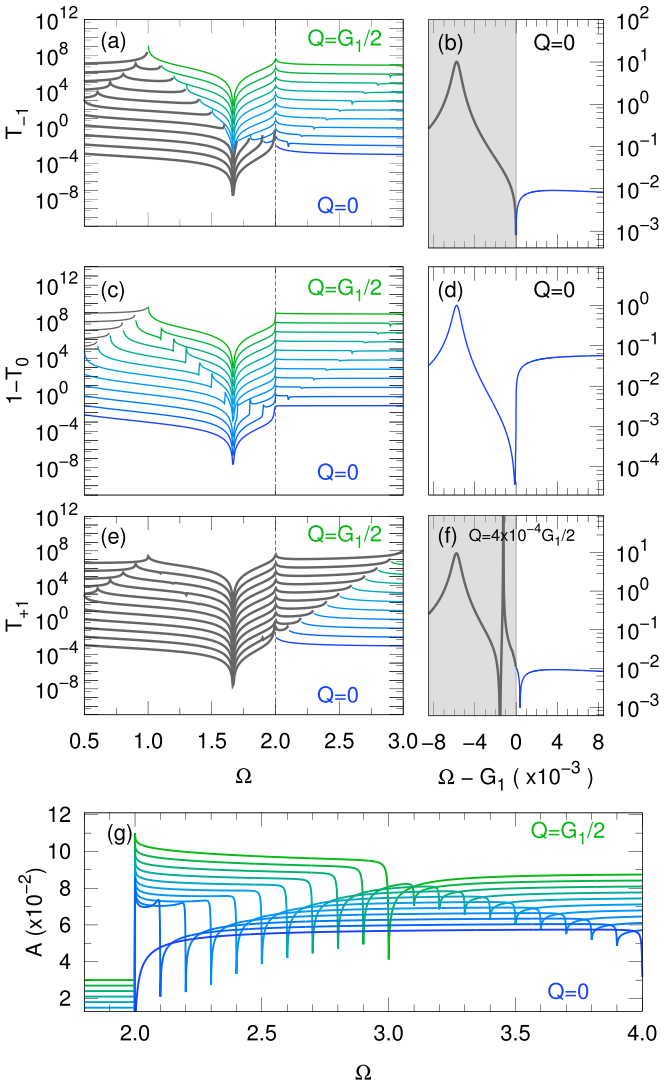

FIG. 12. As Fig. 10 but for $\Delta = 0$ ($G_1 = 2$).

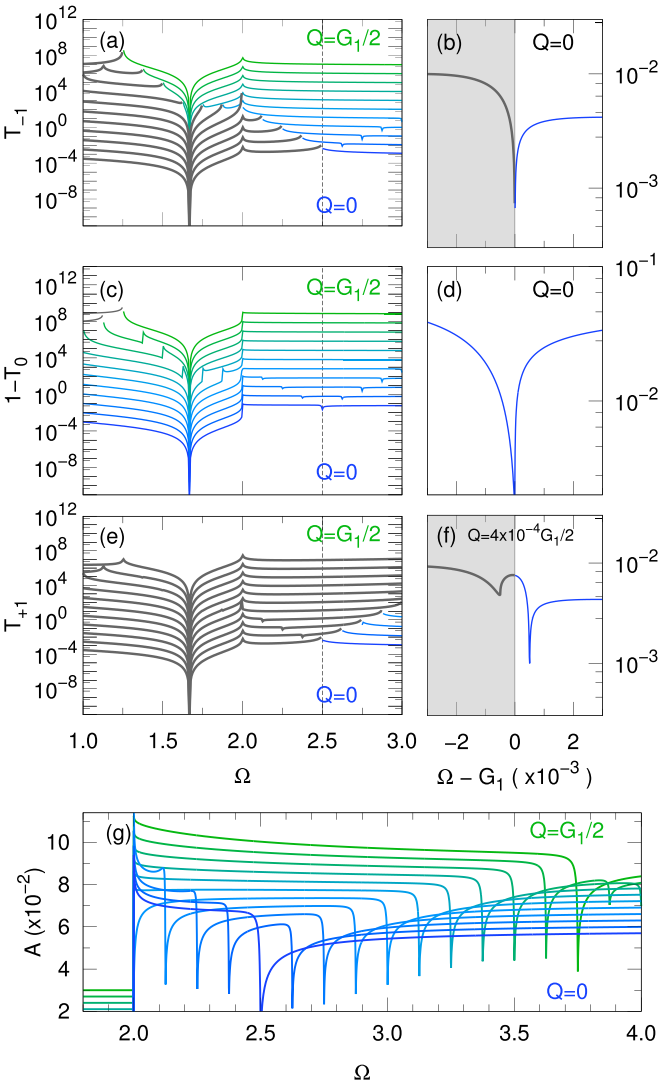

FIG. 13. As Fig. 10 but for $\Delta = 0.5$ ($G_1 = 2.5$).

Since the mode features are sharp in frequency, we show a zoom-in of the TE mode transmission at $Q = 0$ for minus-first [Figs. 7(b), 8(b), and 9(b)] and zeroth [Figs. 7(d), 8(d), and 9(d)] diffraction orders. First order transmission for small but finite Q is shown in Figs. 7(f), 8(f), and 9(f).

For $\Delta = -1$ (Fig. 7), the TE mode dip (not peak) for $Q = 0$ appears at a frequency very close to G_1 [see Fig. 7(b)]. When Q is slightly increased [Fig. 7(f)], the TE mode dip moves away from G_1 increasing in frequency within the open diffraction channel region (not gray).

For $\Delta = -2 + 1.667$ (Fig. 8), the TE mode peak can be also seen moving to higher frequencies for Q slightly increasing from $Q = 0$ [Fig. 8(b)] to $Q \neq 0$ [Fig. 8(f)]. The peak width is very small, about 10^{-10} in this case due to the vanishing graphene conductivity near this frequency of $\Omega \approx 1.667$ [2].

For $\Delta = 0$ (Fig. 9), the TE mode peak is clearly enhanced due to the dip in the imaginary part of the conductivity. The TE SPP peak in the coefficient of the evanescent near field (gray area) moves to lower frequencies for increasing Q from Fig. 9(b) to Fig. 9(f), in agreement with the observations in Fig. 4(a).

2. Turbostratic case

Figures 10–13 show transmission and absorption spectra for turbostratic ($N = 10$) graphene grating for $\Delta = -1$, $-2 + 1.667$, 0, and 0.5, respectively, corresponding to $G_1 = 1$, 1.667, 2, and 2.5. Features related to the mode peaks and interband peaks are qualitatively the same here as in the single-layer case in Appendix B 1 which can be seen by comparing frequencies of peaks (or dips) in panels (a),(c),(e),(g) of Figs. 7–9, to those of same panels of Figs. 10–12, with matching Δ.

The factor of $N = 10$ multiplying the conductivity increases the absorption by the same factor to the order of 10^{-1}. The zoom in Figs. 10(b), 10(d), and 10(f) (and corresponding panels in Figs. 11–13) show effects of this factor in amplitude of peaks and the frequency of peaks and dips moving further away from G_1 by a factor of about 10^2, compared to the single-layer case. Importantly, the zoom in frequency near $\Omega = 2$ in

Figs. 12(b), 12(d), and 12(f) shows evidence of amplification in first and minus-first diffraction orders and attenuation of the transmission in the zeroth diffraction order, compared to that in the single-layer case.

[1] S. A. Mikhailov and K. Ziegler, New electromagnetic mode in graphene, Phys. Rev. Lett. **99**, 016803 (2007).

[2] Z. Ahmad, E. A. Muljarov, and S. S. Oh, Extended frequency range of transverse-electric surface plasmon polaritons in graphene, Phys. Rev. B **104**, 085426 (2021).

[3] S. H. Lee, M. Choi, T.-T. Kim, S. Lee, M. Liu, X. Yin, H. K. Choi, S. S. Lee, C.-G. Choi, S.-Y. Choi, X. Zhang, and B. Min, Switching terahertz waves with gate-controlled active graphene metamaterials, Nat. Mater. **11**, 936 (2012).

[4] D. Zhan, J. Yan, L. Lai, Z. Ni, L. Liu, and Z. Shen, Engineering the electronic structure of graphene, Adv. Mater. **24**, 4055 (2012).

[5] S. Bahadori-Haghighi, R. Ghayour, and A. Zarifkar, Tunable graphene–dielectric metasurfaces for terahertz all-optical modulation, J. Appl. Phys. **128**, 044506 (2020).

[6] Q. Bao, H. Zhang, B. Wang, Z. Ni, C. H. Y. X. Lim, Y. Wang, D. Y. Tang, and K. P. Loh, Broadband graphene polarizer, Nat. Photonics **5**, 411 (2011).

[7] P. S. Maji and R. Das, Absorption enhancement in monolayer graphene using Tamm plasmon polaritons, OSA Continuum **1**, 392 (2018).

[8] Y. Guo, S. Wang, Y. Zhou, C. Chen, J. Zhu, R. Wang, and Y. Cai, Broadband absorption enhancement of graphene in the ultraviolet range based on metal-dielectric-metal configuration, J. Appl. Phys. **126**, 213103 (2019).

[9] X. Y. He, J. Tao, and B. Meng, Analysis of graphene TE surface plasmons in the terahertz regime, Nanotechnology **24**, 345203 (2013).

[10] D. A. Kuzmin, I. V. Bychkov, V. G. Shavrov, and V. V. Temnov, Plasmonics of magnetic and topological graphene-based nanostructures, Nanophotonics **7**, 597 (2018).

[11] D. Jin, T. Christensen, M. Soljačić, N. X. Fang, L. Lu, and X. Zhang, Infrared topological plasmons in graphene, Phys. Rev. Lett. **118**, 245301 (2017).

[12] T. M. Slipchenko, J.-M. Poumirol, A. B. Kuzmenko, A. Y. Nikitin, and L. Martín-Moreno, Interband plasmon polaritons in magnetized charge-neutral graphene, Commun. Phys. **4**, 110 (2021).

[13] M. Taillefumier, V. K. Dugaev, B. Canals, C. Lacroix, and P. Bruno, Graphene in a periodically alternating magnetic field: An unusual quantization of the anomalous Hall effect, Phys. Rev. B **84**, 085427 (2011).

[14] P. A. D. Gonçalves, E. J. C. Dias, Y. V. Bludov, and N. M. R. Peres, Modeling the excitation of graphene plasmons in periodic grids of graphene ribbons: An analytical approach, Phys. Rev. B **94**, 195421 (2016).

[15] L. Cui, J. Wang, and M. Sun, Graphene plasmon for optoelectronics, Rev. Phys. **6**, 100054 (2021).

[16] M. B. Rhouma, B. Guizal, P. Bonnet, F. Paladian, and K. Edee, Semi-analytical model for the analysis of a magnetically biased 1D subwavelength graphene-strip-grating, Opt. Continuum **1**, 1144 (2022).

[17] L. Xiong, C. Forsythe, M. Jung, A. S. McLeod, S. S. Sunku, Y. M. Shao, G. X. Ni, A. J. Sternbach, S. Liu, J. H. Edgar, E. J. Mele, M. M. Fogler, G. Shvets, C. R. Dean, and D. N. Basov, Photonic crystal for graphene plasmons, Nat. Commun. **10**, 4780 (2019).

[18] N. K. Emani, D. Wang, T.-F. Chung, L. J. Prokopeva, A. V. Kildishev, V. M. Shalaev, Y. P. Chen, and A. Boltasseva, Plasmon resonance in multilayer graphene nanoribbons, Laser Photonics Rev. **9**, 650 (2015).

[19] G. Li, V. Semenenko, V. Perebeinos, and P. Q. Liu, Multilayer graphene terahertz plasmonic structures for enhanced frequency tuning range, ACS Photonics **6**, 3180 (2019).

[20] D. Rodrigo, A. Tittl, O. Limaj, F. J. G. de Abajo, V. Pruneri, and H. Altug, Double-layer graphene for enhanced tunable infrared plasmonics, Light Sci. Appl. **6**, e16277 (2017).

[21] H. Yan, X. Li, B. Chandra, G. Tulevski, Y. Wu, M. Freitag, W. Zhu, P. Avouris, and F. Xia, Tunable infrared plasmonic devices using graphene/insulator stacks, Nat. Nanotechnol. **7**, 330 (2012).

[22] M.-D. He, G. Zhang, J.-Q. Liu, J.-B. Li, X.-J. Wang, Z.-R. Huang, L. Wang, and X. Chen, Plasmon resonances in a stacked pair of graphene ribbon arrays with a lateral displacement, Opt. Express **22**, 6680 (2014).

[23] S. Gong, L. Wang, Y. Zhang, Z. Yang, X. Li, Q. Wen, Z. He, S. Liang, L. Yuan, C. Yu, Z. Feng, Z. Yang, and X. Zhang, Ultra-extraordinary optical transmission induced by cascade coupling of surface plasmon polaritons in composite graphene–dielectric stack, Opt. Express **28**, 30502 (2020).

[24] I. Haddouche and L. Cherbi, Comparison of finite element and transfer matrix methods for numerical investigation of surface plasmon waveguides, Opt. Commun. **382**, 132 (2017).

[25] M. Maier, D. Margetis, and M. Luskin, Dipole excitation of surface plasmon on a conducting sheet: Finite element approximation and validation, J. Comput. Phys. **339**, 126 (2017).

[26] J. Jung, T. Søndergaard, and S. I. Bozhevolnyi, Theoretical analysis of square surface plasmon-polariton waveguides for long-range polarization-independent waveguiding, Phys. Rev. B **76**, 035434 (2007).

[27] J. Shibayama, J. Yamauchi, and H. Nakano, Frequency-dependent FDTD analyses of terahertz plasmonic devices, in *2020 International Symposium on Antennas and Propagation (ISAP)* (IEEE, Piscataway, NJ, 2021), pp. 457–458.

[28] T. Zang, H. Zang, Z. Xi, J. Du, H. Wang, Y. Lu, and P. Wang, Asymmetric excitation of surface plasmon polaritons via paired slot antennas for angstrom displacement sensing, Phys. Rev. Lett. **124**, 243901 (2020).

[29] M. Rana, B. Hossain, R. Islam, and Y. G. Guo, Surface plasmon polariton propagation modeling for graphene parallel pair sheets using FDTD, in *2015 IEEE International Conference on Applied Superconductivity and Electromagnetic Devices (ASEMD)* (IEEE, Piscataway, NJ, 2015), pp. 179–180.

[30] J. Olkkonen, FDTD scattered field formulation for scatterers in stratified dispersive media, Opt. Express **18**, 4380 (2010).

[31] T. Weiss, N. A. Gippius, S. G. Tikhodeev, G. Granet, and H. Giessen, Derivation of plasmonic resonances in the Fourier

modal method with adaptive spatial resolution and matched coordinates, J. Opt. Soc. Am. A **28**, 238 (2011).

[32] N. Anttu and H. Q. Xu, Scattering matrix method for optical excitation of surface plasmons in metal films with periodic arrays of subwavelength holes, Phys. Rev. B **83**, 165431 (2011).

[33] G. M. Maksimova, E. S. Azarova, A. V. Telezhnikov, and V. A. Burdov, Graphene superlattice with periodically modulated Dirac gap, Phys. Rev. B **86**, 205422 (2012).

[34] A. Y. Nikitin, F. Guinea, and L. Martin-Moreno, Resonant plasmonic effects in periodic graphene antidot arrays, Appl. Phys. Lett. **101**, 151119 (2012).

[35] C. Wei, R. Negishi, Y. Ogawa, M. Akabori, Y. Taniyasu, and Y. Kobayashi, Turbostratic multilayer graphene synthesis on CVD graphene template toward improving electrical performance, Jpn. J. Appl. Phys. **58**, SIIB04 (2019).

[36] I. H. Baek, J. M. Hamm, K. J. Ahn, B. J. Kang, S. S. Oh, S. Bae, S. Y. Choi, B. H. Hong, D.-I. Yeom, B. Min, O. Hess, Y. U. Jeong, and F. Rotermund, Boosting the terahertz nonlinearity of graphene by orientation disorder, 2D Mater. **4**, 025035 (2017).

[37] R. A. Watts, T. W. Preist, and J. R. Sambles, Sharp surface-plasmon resonances on deep diffraction gratings, Phys. Rev. Lett. **79**, 3978 (1997).

[38] Y. Lu, M. H. Cho, Y. Lee, and J. Y. Rhee, Polarization-independent extraordinary optical transmission in one-dimensional metallic gratings with broad slits, Appl. Phys. Lett. **93**, 061102 (2008).

[39] E. Moreno, L. Martín-Moreno, and F. J. García-Vidal, Extraordinary optical transmission without plasmons: The s-polarization case, J. Opt. A: Pure Appl. Opt. **8**, S94 (2006).

[40] S. Maier, *Plasmonics: Fundamentals and Applications* (Springer, Berlin, 2007).

[41] L. A. Falkovsky, Optical properties of graphene, J. Phys.: Conf. Ser. **129**, 012004 (2008).

[42] D. M. Whittaker and I. S. Culshaw, Scattering-matrix treatment of patterned multilayer photonic structures, Phys. Rev. B **60**, 2610 (1999).

[43] S. G. Tikhodeev, A. L. Yablonskii, E. A. Muljarov, N. A. Gippius, and T. Ishihara, Quasiguided modes and optical properties of photonic crystal slabs, Phys. Rev. B **66**, 045102 (2002).

[44] D. A. Bykov and L. L. Doskolovich, Numerical methods for calculating poles of the scattering matrix with applications in grating theory, J. Lightwave Technol. **31**, 793 (2013).

[45] A. B. Akimov, A. S. Vengurlekar, T. Weiss, N. A. Gippius, and S. G. Tikhodeev, Surface plasmon polaritons in metallo-dielectric meander-type gratings, JETP Lett. **90**, 355 (2009).

[46] H. Min and A. H. MacDonald, Electronic structure of multilayer graphene, Prog. Theor. Phys. Suppl. **176**, 227 (2008).

[47] J. A. Garlow, L. K. Barrett, L. Wu, K. Kisslinger, Y. Zhu, and J. F. Pulecio, Large-area growth of turbostratic graphene on Ni(111) via physical vapor deposition, Sci. Rep. **6**, 19804 (2016).

[48] R. Negishi, K. Yamamoto, H. Kitakawa, M. Fukumori, H. Tanaka, T. Ogawa, and Y. Kobayashi, Synthesis of very narrow multilayer graphene nanoribbon with turbostratic stacking, Appl. Phys. Lett. **110**, 201901 (2017).

[49] B. Bolotovskii and A. Lebedev, On threshold phenomena in classical electrodynamics, Zh. Eksp. Teor. Fiz. **53**, 784 (1967) [Sov. Phys. JETP **26**, 784 (1968)].

[50] C. C. Wojcik, H. Wang, M. Orenstein, and S. Fan, Universal behavior of the scattering matrix near thresholds in photonics, Phys. Rev. Lett. **127**, 277401 (2021).

[51] T. Fujita, Y. Sato, T. Kuitani, and T. Ishihara, Tunable polariton absorption of distributed feedback microcavities at room temperature, Phys. Rev. B **57**, 12428 (1998).

[52] A. Yablonskii, E. Muljarov, N. Gippius, S. Tikhodeev, T. Fujita, and T. Ishihara, Polariton effect in distributed feedback microcavities, J. Phys. Soc. Jpn. **70**, 1137 (2001).

[53] Z. Ahmad, S. S. Oh, and E. Muljarov, Transmission spectra data of periodically modulated graphene structure, Cardiff University (2024), http://doi.org/10.17035/d.2024.0310746010.